Advances in Science and Technology Research Journal

Advances in Science and Technology Research Journal, 2026, 20(4), 145–159
https://doi.org/10.12913/22998624/214674
ISSN 2299-8624, License CC-BY 4.0

Received: 2025.10.24
Accepted: 2026.02.15
Published: 2026.03.01

The role of two-stage powders mixing and tungsten element on mechanical and electrical properties of the CuNiFe-xW alloys

Suprianto[1*], M. Rafli[1], Ardy Afriandy Ginting[1], Sutrisna[2], Ali Hanafiah Rambe[3]

[1] Department of Mechanical Engineering, Faculty of Engineering, Universitas Sumatera Utara, Jl. Almamater Kampus USU, Medan, 20155, Indonesia
[2] Department of Mechanical Engineering, Faculty of Engineering and Planning, Institut Teknologi Nasional Yogyakarta 55281, Indonesia
[3] Department of Electrical Engineering, Faculty of Engineering, Universitas Sumatera Utara, Jl. Almamater Kampus USU, Medan, 20155, Indonesia
* Corresponding author's e-mail: suprianto@usu.ac.id

ABSTRACT

Cu-based alloys are extensively utilized in engineering applications, including electrodes for electrical components. The combination of both transition and refractory elements is a promising candidate for this application due to their superior ductility and strength at elevated temperatures. This study examines the influence of (W, Fe) pre-milling time and the (x=1, 3, 5, 7) wt.%W element on the characteristics of CuNiFe-xW alloys synthesized by powder metallurgy through a two-stage powder mixing process. The initial stage involved the mixing of (W, Fe) powders through pre-milling utilizing planetary ball milling for durations of 0.5, 1.0, 2.0, and 4.0 h, maintaining a ball to powder ratio (BPR) of 10:1. The second mixing stage entails the mixing of (W, Fe) and (Cu, Ni) powders by using a V-mixer for 120 minutes at low velocity, followed by cold compaction and high-temperature sintering, the characteristics of sintered CuNiFe-xW alloys were assessed through mechanical and electrical tests at ambient temperature. Microstructural analyses, fracture morphologies, and elemental distributions in the sintered model CuNiFe-xW alloys were performed using a scanning electron microscope (SEM) and Energy Dispersive Spectroscopy (EDS) at various magnifications. The crystal structure of CuNiFe-5 wt.%W alloys in both powder and bulk forms was analyzed using the X-ray diffraction method (XRD). Furthermore, the electrical properties of the model CuNiFe-xW alloys were measured using the four-probe measurement method. The findings indicate that the inclusion of W and (W, Fe) pre-milling markedly improves the hardness and compressive yield strength of model CuNiFe-xW alloys. The augmentation of pre-milling durations for (W, Fe) powders diminishes the crystallite size, enhances uniform particle distribution, and elevates electrical conductivity. It is clear that the addition of W and the implementation of (W, Fe) pre-milling positively influence strength; nevertheless, the presence of W tends to reduce the electrical conductivity of the CuNiFe-xW alloys.

Keywords: alloys, compressive strength, electrical conductivity, hardness, pre-milling.

INTRODUCTION

Powder metallurgy (PM) is a potential approach for synthesizing a wide range of metal alloys. Copper (Cu), ceramic particles, and refractory materials with different melting points can be synthesized by the PM method. This technique also resulted in more homogeneous elemental distribution. On the other hand, the elemental segregation that occurred in the alloys synthesized by casting was reported [1, 2]. Furthermore, the Cu matrix composite reinforced with Al-Oxide and Ti particles was effectively synthesized by PM [3]. The incorporation of refractory elements such as W into Cu-3 wt.%Si [4] and Mo in the Al-Cu alloys [5] significantly enhances the strength of the alloys. The addition of W improved the strength of the Ni alloys through a solid solution [6], the development of the Fe7W6 intermetallic phase [7], and

the in-situ formation of WC/W2C carbides [8]. These mechanisms exert varying influences on the compressive strength, yield strength, hardness, and ductility of the alloys. On the other hand, the addition of Fe into Cu-Ni-Mn alloy increases hardness and generates precipitate formation [9]. This element also contributed to improving the hardness of the Cu-Ni [10]. Even though the Fe element facilitated grain refining and strengthening effects, it diminished the electrical conductivity of Cu-Fe alloys [11]. Both W and Fe are essential for enhancing the strength of the alloys. Nonetheless, the strengthening process primarily considers the particle size and their distribution; a finer phase of Fe contributes to the mechanical strength of the Cu-Fe alloys wire [12]. A fine particle size and uneven shape enhance the electrical conductivity of the Cu [13]. While finer particles enhance alloy properties, ensuring uniform dispersion and minimizing agglomeration poses significant challenges in powder technology. The mixing process is essential for attaining a homogeneous particle dispersion and enhanced mechanical properties. A barrel mixer and V-blender were used to synthesize the aluminum composite; the mechanical properties are affected by process settings [14]. The V-mixer type exhibits a uniform particle dispersion and a straightforward operating system [15]. The characteristics of the W-Cu alloy are influenced by both distribution and particle size [16]. A refined particle Fe-Ni alloy obtained by mechanical alloying is reported [17]. The Cu-Fe pre-milling followed by mechanical alloying shows an FCC solid solution formed [18]. This process has also been done for different characteristic elements, which promotes the fine Mo dispersed within the Cu matrix [19], increases the amount of Mn in the Al-Mn-Cu, smaller lattice parameter and hardness improvement [20]. It is clearly reported that the powder pre-milling influences the particle size and the characteristics of the alloys. Furthermore, the fine-grained and carbide particle size enhances the tensile strength of the CuCrFeNi alloys [21]. The strength and electrical conductivity improvement of the Cu-Cr alloy is closely linked to the formation of fine Cr precipitates and the reduction of solid-solute Cr, respectively [22]. It is believed that the composition and mixing models play an important role in the microstructure evolution. The increasing milling speed and the addition of an additive reduced the W particle size [23]. A long milling time promotes a finer microstructure of the Cu-Fe-Co-W alloy [24], and a homogeneous distribution of the B4C particles within the microstructure of the Cu-B4C obtained [25]. Milling time and ball-to-powder ratio are essential for reducing the particle size of the Cu25W alloy [26]. Prevailing research indicates that mixing models and the incorporation of refractory components are critical variables in enhancing the characteristics of Cu alloys produced by powder metallurgy.

Furthermore, the related work from previous studies investigated the role of W, Fe, and the mixing model on the mechanical and electrical properties of the Cu based alloy was carried out partially. In which the pre-milling process is limited to Cu-Fe, Cu-Mo, and Mn powders. Thus, the effect of the combination of both W element and (W, Fe) powder pre-milling to obtain a balance between good mechanical and electrical properties of the Cu-Ni-based alloys is still challenging. In the current work, the focus is on investigating the effects of the individual W elements and two-stage (W, Fe) mixing with different pre-milling durations on the electrical and mechanical properties of Cu-Ni-based alloys.

MATERIALS AND METHODS

The synthesis of CuNiFe-xW alloys using the powder metallurgy technique was carried out, with high-purity metal powders (>99.90%) and 30-40 μm particle sizes as starting material in the current study. A starting element comprises Cu, Ni, Fe, and xW, in which x = 1.0, 3.0, 5.0, and 7.0 wt.% of the W element. These alloys are designated as (1–4) A and (5-8) B model alloys, as demonstrated in Table 1. The powders are mixed into the cane using a Glove Box in an Argon atmosphere to prevent excessive contamination. Furthermore, powder mixing using a V-mixer was conducted to obtain a homogeneous distribution of these particles in the absence of a pre-milling process. On the other hand, the CuNiFe-5.0 wt.%W powders were mixed thoroughly in two stages, consisting of (W, Fe) powders pre-milled using mechanical alloying, equipped with a cane and grinding media made from hard material. The process parameters include a speed of 1.000 rpm, the ball-to-powder ratio (BPR) 10:1, and the (W, Fe) powder pre-milling time 0.5, 1.0, 2.0, and 4.0 h. In the second stage, both

(W, Fe) pre-milled and (Cu, Ni) powder were placed into a V-mixer at a speed of 120 rpm for 2 h to obtain a homogeneous distribution of the constituent elements.

The mixing of pre-milled (W, Fe) with (Cu, Ni) elements by using a V-mixer with similar parameters to model alloys "A" and they are referred to as number (5–8) B model alloys, see Table 1. The green compact of the CuNiFe-xW alloys was generated using cold compaction at a penetrating force of 250 MPa for 15 minutes. Moreover, high-temperature sintering at 770 °C for 60 h duration by using a muffle furnace was used to achieve the maximum densification of the bulk model alloys. In this current study, the sintering temperature is about 71% of the melting point of the Cu matrix. Based on the Cu-Ni phase diagram, these elements are in the solid phase during sintering. The mechanical properties of the sintered alloys were evaluated by a compressive yield strength test with a maximum load capacity of 300 kN and a loading rate of 5 mm/min, alongside a Vickers hardness test utilizing a 100 g load for a 5 s penetration time. The electrical properties, which consist of electrical conductivity and resistivity, were measured by a Keithley model machine with three measurements. Both the mechanical and electrical properties were measured at room temperature. The microstructure and fracture morphologies were observed by using an SEM and EDS to analyze the component elements and their distribution in the microstructure of the CuNiFe-xW model alloys. The crystal structure and phases formed in the powder stage and sintered alloys were characterized by the X-ray diffraction method with Cu-Kα.

RESULTS AND DISCUSSION

The SEM images of the CuNiFe-5.0W powders stage

Figure 1 shows the SEM image and EDS results of the powder stage of the CuNiFe-5.0W alloys with 0.5 h (W, Fe) pre-milling. The model alloys' powder stage is mostly composed of Cu elements, with a sponge shape and a size of less than 40 µm. Aside from Cu, the (Ni, Fe, and W) elements with smaller particle size and irregular shape are scattered throughout the Cu particle, clearly observed. The EDS spectra and amount of each constituent component consist of 84.7 wt.%Cu, 7.2 wt.%Ni, 1.8 wt.%Fe, and 6.3 wt.%W. This finding suggests that the milled powder compositions are similar to those of Cu-based alloys (see Table 1). This result demonstrates a uniform dispersion of particles during the pre-milling and subsequent V-mixer operation. However, only a small amount of impact energy is imparted to the powder mixed by the V-mixer and ball grinding media, resulting in no substantial changes in Cu particle size or shape. A 2.0-hour (W, Fe) pre-milling was performed to provide a finer and more uniform dispersion of (W, Fe) particles inside the (Cu, Ni) matrix. Figure 2 shows the particle distribution of the mixed powders after 2.0 h of pre-milling with (W, Fe) powder.

Figure 1 shows a sponge-like structure with irregularly shaped particles after 2.0 h of (W, Fe) pre-milling. However, smaller W particles (less than 20 µm) were also formed, attributable to the (W, Fe) powder pre-milling procedure. These findings demonstrate that mechanical alloying before

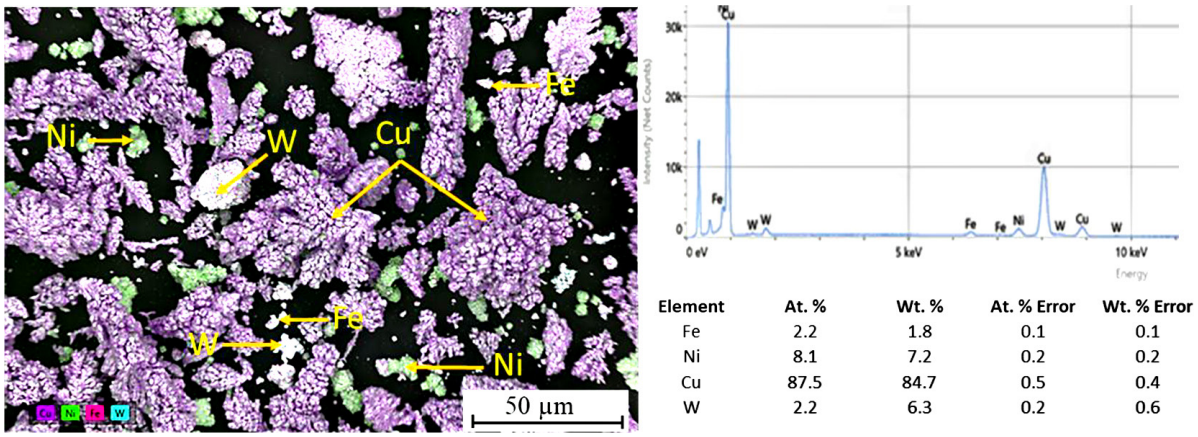

Element	At. %	Wt. %	At. % Error	Wt. % Error
Fe	2.2	1.8	0.1	0.1
Ni	8.1	7.2	0.2	0.2
Cu	87.5	84.7	0.5	0.4
W	2.2	6.3	0.2	0.6

Figure 1. SEM image and EDS result of the powder stage of the CuNiFe-5.0W with 0.5 h (W, Fe) pre-milling time, followed by horizontal milling for 2 h

Table 1. The design of the composition of Cu-based alloys and the mixing model

Alloys number	Alloys designation	Composition (wt.%)			Mixing process	
		Fe	W	(90Cu10Ni)	Pre-milling (h)	V-mixer
1-A	CuNiFe-1.0W	2.5	1.0	Balance	-	√
2-A	CuNiFe-3.0W	2.5	3.0	Balance	-	√
3-A	CuNiFe-5.0W	2.5	5.0	Balance	-	√
4-A	CuNiFe-7.0W	2.5	7.0	Balance	-	√
5-B	CuNiFe-5.0W-P0	2.5	5.0	Balance	0.5	√
6-B	CuNiFe-5.0W-P1	2.5	5.0	Balance	1.0	√
7-B	CuNiFe-5.0W-P2	2.5	5.0	Balance	2.0	√
8-B	CuNiFe-5.0W-P3	2.5	5.0	Balance	4.0	√

milling reduces element particle sizes (W, Fe). It has also been reported that mechanical alloying of ODS ferritic steel powder causes a decrease in particle size [21]. The combined powder contains elements (Cu, Ni, Fe, and W), as demonstrated by the EDS spectra and component quantities in Figure 2. These elements correspond to the design given in Table 1. This indicates that powders blended using the V-mixer provide uniform particle distribution. Furthermore, a 2.0-hour (W, Fe) pre-milling procedure with mechanical alloying reduces particle size because strong impact energy repeatedly fractures particles during pre-milling. Milling time influences the particle size of Cu-Ni-Zr alloys, and particle refining involves fracturing that depends on the duration of ball milling [22].

The XRD spectra of the CuNiFe-xW powders

In the current investigation, increasing the (W, Fe) pre-milling time causes a modest decrease in the crystallite size of the CuNiFe-5.0W alloy from 25.7 nm to 19.5 nm, as shown in Figure 3. The (W, Fe) powder pre-milling with high impact energy is thought to have greatly reduced the crystallite size of the alloys. The CuNiFe-5.0W model is mostly composed of (Cu, Ni) components (> 90 wt.%), which were mixed using a V-mixer with a 5:1 ball-to-powder ratio. The minimal impact energy of this procedure results in just a tiny drop in crystallite size. Pre-milling (W, Fe) powder by ball milling can reduce particle size, fracture, deformation, and cold-welding, resulting in a linear increase in lattice strain of up to ±0.49 (%) for 4 h (Figure 3).

In this current study, four elements (Cu, Ni, Fe, and W) were utilized as starting materials; the XRD spectra of the powder with varied (W, Fe) pre-milling are shown in Figure 4. The crystallographic plane is mostly made up of (111), (200), and (220), which are identical to the FCC structure of Cu and Ni elements. These elements also show an overlapping peak for the (111) crystalline plane, indicating that they have comparable characteristics with the ability to form a solid solution phase. In the powder stages, the (110) crystal plane was observed at 2-Theta ±

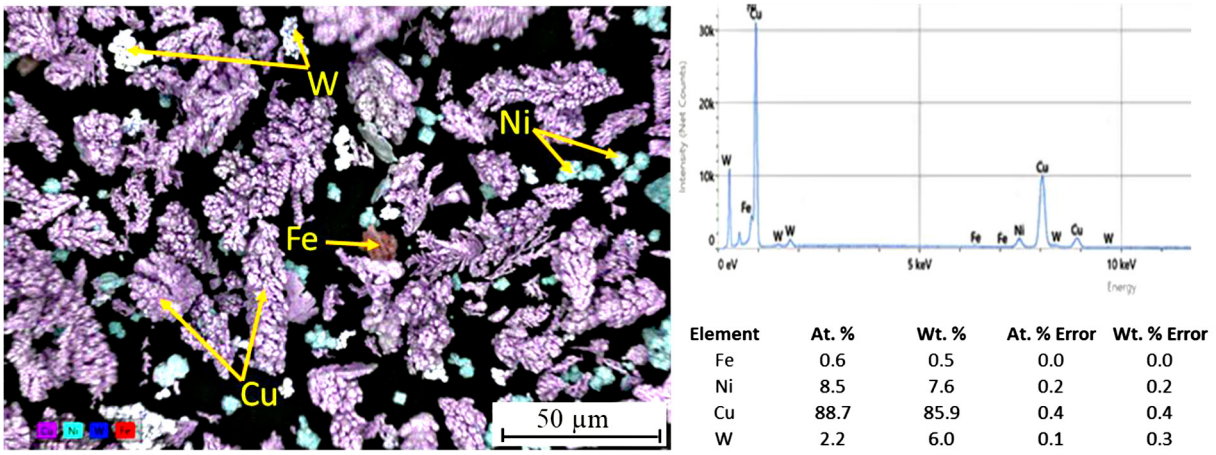

Element	At. %	Wt. %	At. % Error	Wt. % Error
Fe	0.6	0.5	0.0	0.0
Ni	8.5	7.6	0.2	0.2
Cu	88.7	85.9	0.4	0.4
W	2.2	6.0	0.1	0.3

Figure 2. SEM image and EDS result of the powder stage of the CuNiFe-5.0W with 2.0 h (W, Fe) pre-milling time

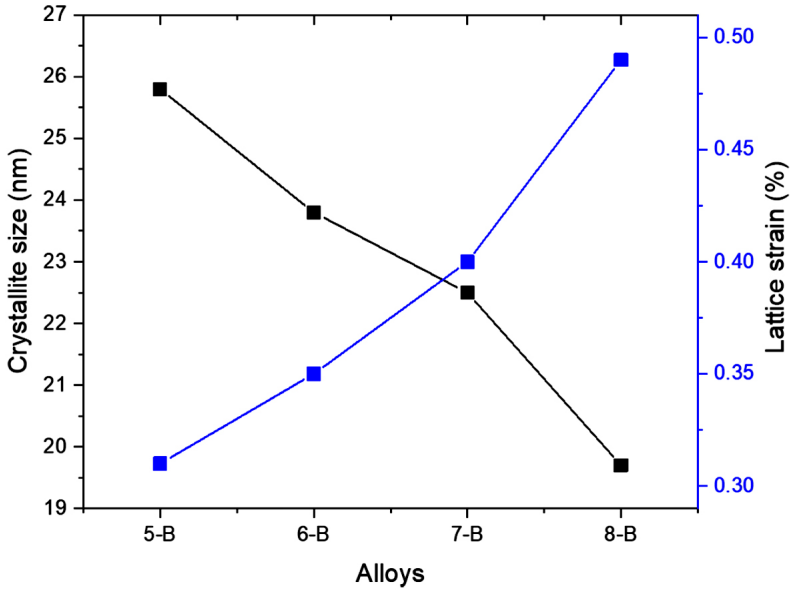

Figure 3. The crystallite size and lattice strain of the CuNiFe-5.0W with different (W, Fe) pre-milling time from 0.5~4.0 h

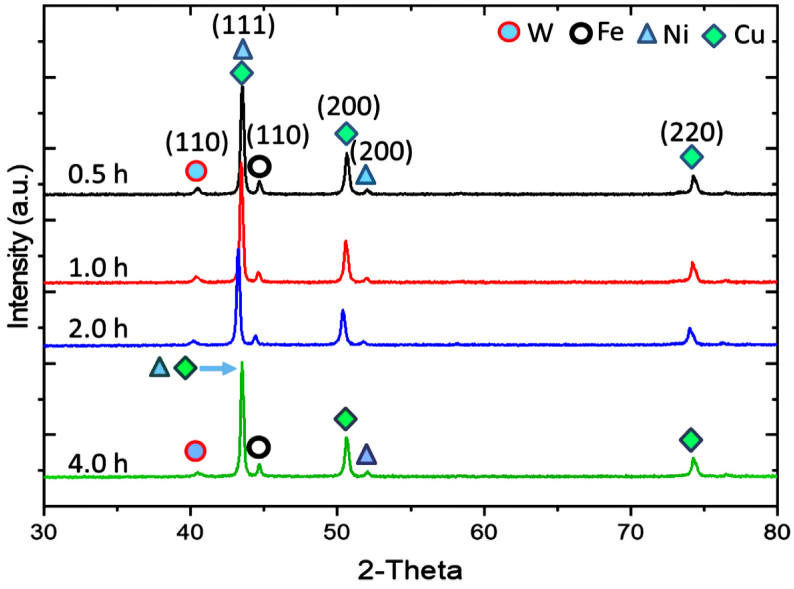

Figure 4. XRD spectra of the CuNiFe-5.0W with different (W, Fe) pre-milling times

41° and 45°, which correspond to the BCC structure of the W and Fe elements, respectively. The (W, Fe) pre-milling promoted the XRD peaks evolution, particularly for the W and Fe peaks, which tend to broaden and slightly decrease in intensity with increasing pre-milling time from 0.5 to 4.0 h. The peak change is believed to be strongly correlated with the reduction in crystallite size, as shown in Figure 3. The decrease in intensity, crystallite size, and peak broadening caused by the mechanical alloying process was also reported to occur in some alloys, such as CoFeNiCrCu and CoCrCuFeMnNix powder [27]. Figure 5 shows the XRD spectra of the CuNiFe-xW model alloys with different tungsten contents (1.0~7.0) wt.%. The addition of the W elements, which have a high atomic weight, contributed to the increase in peak intensity. The maximum peak intensity was found for 7.0 wt.%. W plainly seen, the peak location does not vary considerably, most likely due to the powders being mixed using the V-mixer mixing model at low speed, which does not have sufficient impact energy to refine the particle size significantly.

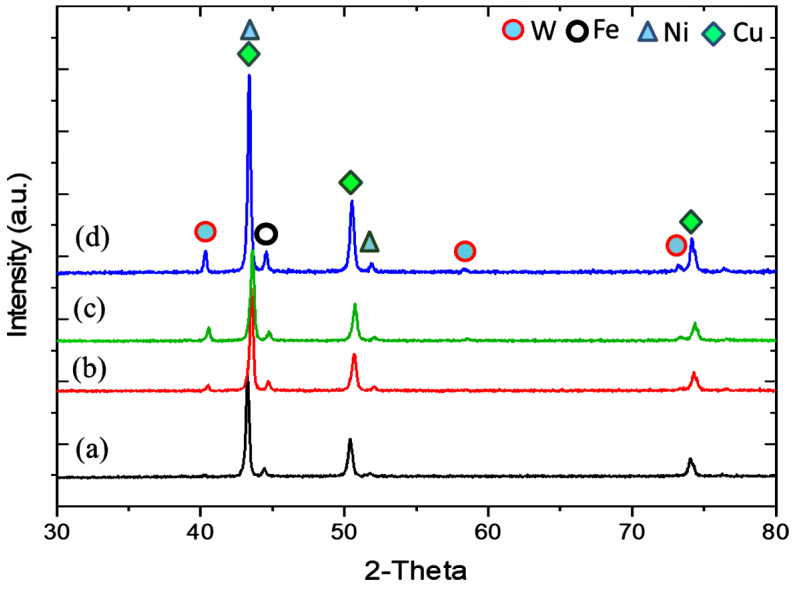

Figure 5. The XRD spectra of the CuNiFe-xW powders with different wt.% W element; (a) 1.0 wt.%, (b) 3.0 wt.%, (c) 5.0 wt.%, and (d) 7.0 wt.%

The microstructure observation

Figure 6 depicts SEM images of several model CuNiFe-xW alloys created using the V-mixer model and (W, Fe) pre-milling. The microstructure of the model alloys CuNiFe-(1, 7) wt.%W was clearly found to consist of a CuNi-rich phase that functions as the matrix in these model alloys, as well as partial Fe-rich particles segregated within the CuNi matrix (Figure 6a-b). Figure 6b shows that the W elements are scattered among CuNi-rich phases, which are characterized as a light gray region with a coarse structure. The microstructure analysis reveals a micro-porosity of less than 10 µm between the major CuNi-rich phases. Porosity development may be caused by

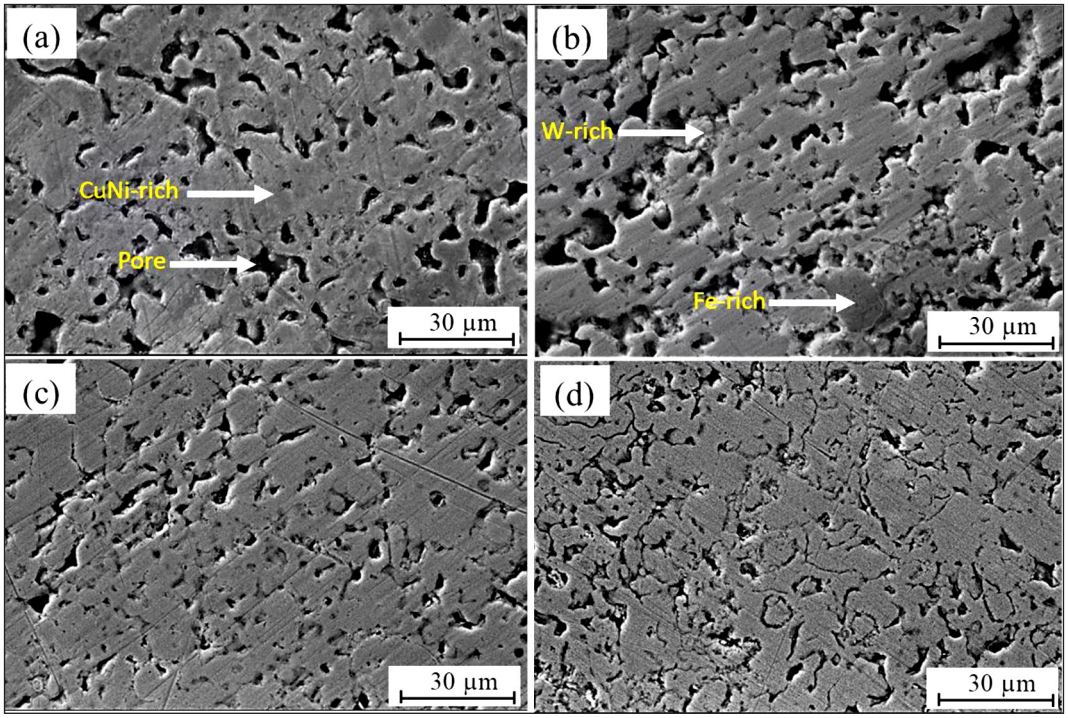

Figure 6. SEM images of different model alloys; (a) CuNiFe-1.0W, (b) CuNiFe-7.0W, (c) CuNiFe-5.0W-P0, and (d) CuNiFe-5.0W-P4

the presence of gas or impurities that become trapped during processing. The involvement of gas and inadequate melt in generating porosity development between the microstructure in copper spheres and aluminum alloys has also been observed [28]. On the other hand, the microstructure of the CuNi-based alloys through (W, Fe) pre-milling for 0.5 h and 4.0 h milling was observed by SEM images, as shown in Figure 6c-d. It was clearly observed that a finer microstructure with oxides and porosities less than 5 µm in size was dispersed between the CuNi-rich phases. The pre-milling of two elements (W, Fe) resulted in a smaller particle size, which is capable of generating more nucleation sites during high-temperature sintering, thereby refining the metal oxide and microstructure of the model alloy.

Furthermore, the constituent elements of the selected areas of the CuNiFe-xW alloys with different wt.% W was investigated, see Figure 7a-b. The areas with different phases, such as CuNi-rich phases, oxides, and porosities, were selected for analysis using the EDS method. Each of the compositions of these phases is shown in Table 2. In Figure 7, point A is the CuNi-rich phase, which consists of 87.4 and 7.3 wt.% of Cu and Ni, respectively. This area is the CuNi solid solution; due to solubility limits cause only a small amount of Fe and W is dissolved into the Cu-Ni-rich phase. At point B, the Cu and Ni elements are not significantly different from point A, indicating a similar phase. A higher oxygen content (7.2 wt.%) was also detected in point B, which is close to the dark particles (Figure 7a).

Point C which is identified as the light gray area, consists of CuNi-rich phase and a slight increase of the W element observed at this point (see Table 2). The W element has the highest melting temperature among constituent elements, and the BCC structure tends to segregate near the grain boundaries of the CuNi-rich phase. This element can act as a reinforcement particle within the Cu-Ni matrix and barriers to dislocation movement.

The constituent elements of the selected area of the model CuNiFe-0.7 wt.%W alloy are shown in Figure 7b and Table 2. Point D, designated as a solid solution phase, has higher concentrations of Cu, Ni, and W; however, this point also detected a significant amount of C elements. Point C is not an expected constituent element due to its acting as a contaminant in these model alloys. The presence of this element might originate from the grinding media during the pre-milling process. A light dark particle with ±10 µm in size (Point E) contains 73.1 wt.%Fe with a low concentration of the Cu, Ni, and W elements. This result also

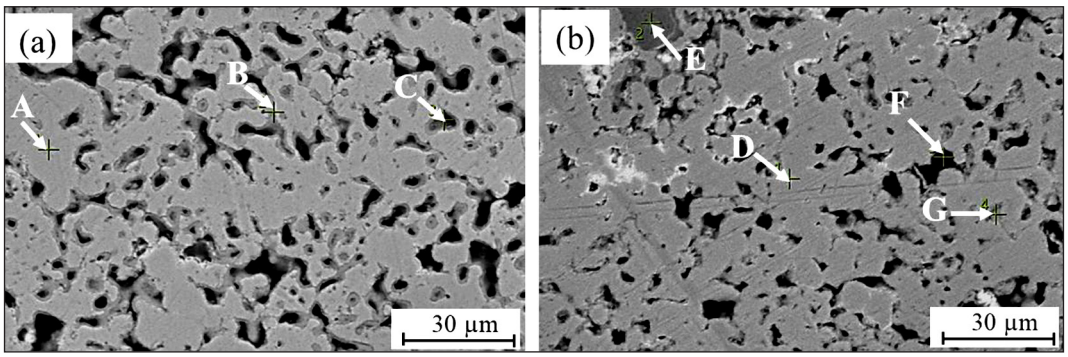

Figure 7. SEM and EDS spectra of the sintered model alloys: (a) CuNiFe-1 wt.%W, and (b) CuNiFe-7 wt.%W

Table 2. The constituent elements selected in the area of the Cu-Ni-Fe-xW in Figure 7

Elements	Composition selected area (wt.%)						
	Point A	Point B	Point C	Point D	Point E	Point F	Point G
Cu	87.4	82.6	85.7	75.6	1.9	48.1	73.4
Ni	7.3	7.3	9.3	6.9	0.5	6.2	8.4
Fe	0.2	0.0	0.0	0.0	73.1	0.2	0.3
W	2.3	2.9	4.0	4.4	0.4	9.0	11.7
O	2.8	7.2	1.0	0.3	24.1	36.5	6.2
C	-	-	-	12.8	-	-	-

confirmed that Fe can be segregated within the microstructure. At this location, the O was found over the (Cu, Ni) elements associated with Point E, which was very close to the porosity area (see Figure 7b). Point F is the area near the porosity with the highest oxygen content (36.5 wt.%), and a significant amount of W (9.0 wt.%) was detected by the EDS method. Point G in Figure 7b is the light gray area, which shows a higher W element content, approximately 11.7 wt.%, dispersed throughout the CuNi matrix.

Figure 8 shows the SEM and EDS mapping of the model CuNiFe-5wt.%W-P0 alloy with 0.5 h (W, Fe) pre-milling time. Within the microstructure of the sintered model alloy, the SEM picture (Figure 8a) clearly reveals the solid solution phase with Cu-Ni-rich elements and a small number of micro-pores linked to dark particles. In the microstructure as a whole, Cu is the principal element. To create a solid solution with Ni elements, this particle is mainly dispersed in the matrix area, as illustrated in Figure 8b-c. There is some segregation of Ni and Fe particles within the microstructure, although the Ni and Cu elements are in proximity to one another (as seen inside the circle in Figure 8b-c). Ni does not always dissolve in Cu, and in fact can be found segregated at the grain boundary of Cu-containing materials [29]. Furthermore, a clustered W-rich phase was observed in the microstructure of sintered CuNiFe-5wt.%W with 0.5 h of (W, Fe) powder pre-milling, as shown in Figure 8e. This fact confirms that the short pre-milling time is insufficient to refine and homogenize the W distribution in the microstructure; this result corresponds to the SEM image of powder distribution (see Figure 1). On the other hand, the oxide particles were also detected by EDS mapping; this element promotes the formation of some clustered areas, particularly concentrated near the porosities, as shown in Figure 8f. Based on the SEM-EDS observation in Figure 8(d-f), it is clearly visible that the O, W, and Fe elements are found in a similar area in the microstructure, which suggests that the formation of some Fe-oxide and W-oxide might be formed in this area for the sintered model CuNiFe-5wt.%W-P0 alloy with 0.5 h (W, Fe) pre-milling times.

Figure 9 displays the EDS mapping of the CuNiFe-5 wt.% W with a 4.0 h (W, Fe) pre-milling period. It became evident that the Cu element becomes uniformly distributed within the microstructure and functions as a matrix in this model alloy when the pre-milling time is increased to 4.0 h. However, some Ni elements still form some clustered particles within the microstructure, as shown in Figure 9c. Furthermore, after 4.0 h of pre-milling, the distribution of (W, Fe) elements appears slightly different. Figure 9d shows that the W particles become finer and more uniformly distributed due to the high-impact energy used in planetary ball milling. Numerous investigations have documented the function of mechanical alloying in WC-Co particle size reduction [30].

On the other hand, the higher pre-milling time resulted in more oxygen being dissolved

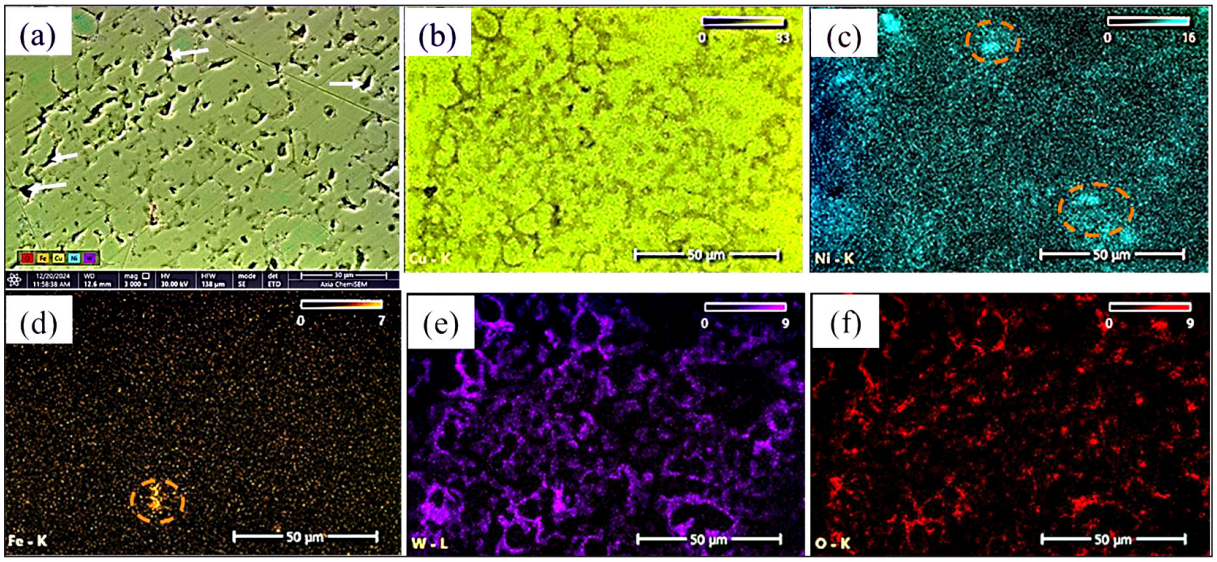

Figure 8. (a) SEM image and constituent elements distribution of the (b) Cu map, (c) Ni map, (d) Fe map, (e) W map, and (f) O map of the CuNiFe-5wt.%W with 0.5 h of the (W, Fe) pre-milling

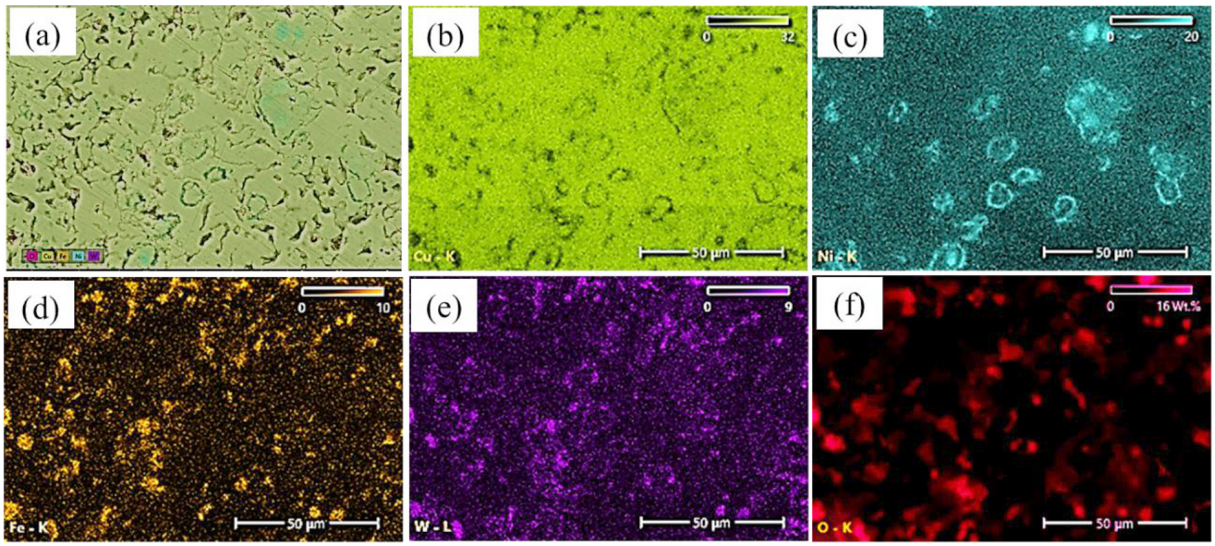

Figure 9. (a) SEM image and distribution of constituent elements of the (b) Cu map, (c) Ni map, (d) Fe map, and (e) W map and (f) O map of the CuNiFe-5wt.%W with 4.0 h pre-milling (Fe, W) powder

into the microstructure, in which the O element concentrates near the pores and Fe-W-rich phase areas. This finding confirms that W-O and Fe-O probably formed in the microstructure of the sintered CuNiFe-5wt.%W. It is believed that Fe has a better affinity with oxygen than Cu and Ni in this model alloy; this condition makes the elements promote metal oxide formation during high-temperature sintering. The amount of each constituent element of model CuNiFe-5wt.%W alloys with 0.5 h and 4 h pre-milling times is shown in Table 3.

Table 3 clearly demonstrates that the increased pre-milling time shows a better elemental distribution, in which the composition of Fe and W is near the alloy design (Table 1). In this current study, a long duration pre-milling causes only a slight increase in the O content from 1.2 to 1.6 wt.% dissolved into powders. The presence of O might generate some metal oxide during high-temperature sintering, which potentially reduces the mechanical and electrical properties. However, the effect of oxides on these characteristics is complicated to explain due to many other factors that contribute to the properties of the alloys.

The XRD spectra of the sintered CuNiFe-5wt.%W alloy

Figure 10 shows the XRD spectra of sintered model CuNiFe-5wt.%W alloys with 4.0 h (W, Fe) pre-milling times. It is clearly detected that the model alloys mainly consist of (111), (200), and (220) crystal planes, which are associated with the FCC phase and correspond well with the Cu-Ni matrix, as shown in Table 1. Intersecting peaks with FCC also revealed the presence of the Cu individual element. Fe and W can likely dissolve into the FCC matrix in modest amounts because of the BCC structure and strong affinity with oxygen. However, the formation of Fe-oxides (Fe_2O_3) and W-oxide (W17O47) has been identified as an overlapping peak at the 2-Theta angle of about 31.13° and FeO was also detected at 36.06°, as shown in Figure 10.

The Fe-oxide formation was confirmed by the EDS point, which detected Fe, W, and O in a similar area within the microstructure, as shown in points E and F (see Figure 7). As seen in Figure 10, the sintered CuNiFe-5 wt.% W alloy retains the locations and phases of the peaks with only slight variations in peak intensity after undergoing the 4.0 h (W, Fe) powders pre-milling

Table 3. The constituent elements mapping areas of the Cu-Ni-Fe-W in Figures 8 and 9

(W, Fe) pre-milling time	Composition of mapping area Cu-Ni-Fe-5 wt.%W				
	Cu (wt.%)	Ni (wt.%)	Fe (wt.%)	W (wt.%)	O (wt.%)
0.5 h	80.1	8.7	0.3	9.7	1.2
4.0 h	82.8	8.0	1.3	6.3	1.6

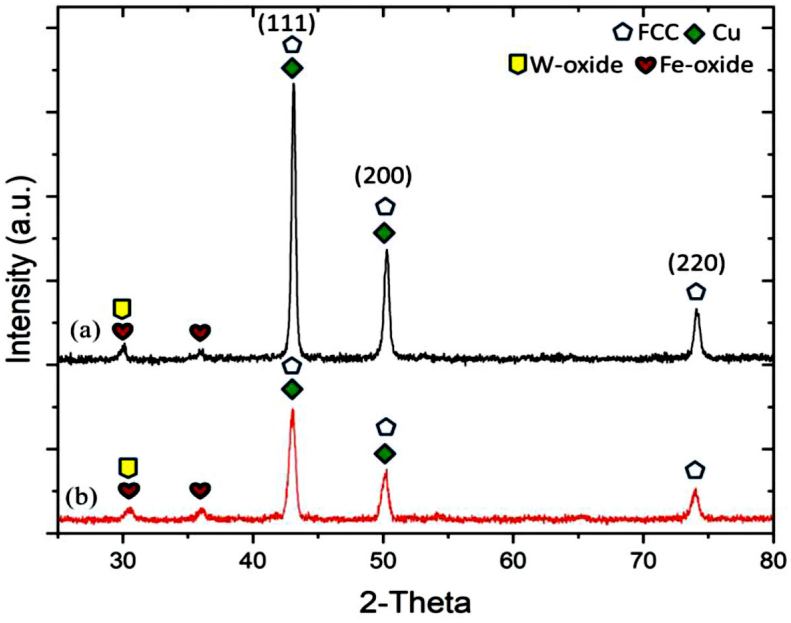

Figure 10. XRD spectra of the sintered CuNiFe-5 wt.%W alloy with (a) 4 h (W, Fe) pre-milling time and (b) without (W, Fe) pre-milling

process. The higher peak intensity may correlate with a better crystalline structure of the material obtained after a high-temperature process [31].

The mechanical properties of the sintered CuNiFe-xW alloys

The mechanical properties of the sintered model alloys were characterized by Vickers hardness and compression tests, as shown in Table 4. The increase in hardness with the increase in W content was observed for alloy numbers 1-A to 4-A, with a hardness of 83 HV obtained for CuNiFe-7 wt.% W (1-A). The addition of W elements to Cu-Ni-Fe alloys increases their hardness, as is readily apparent. Reportedly, W had a comparable impact on the Cu-Fe alloy, enhancing its hardness, wear resistance, and microstructure evolution [32]. Furthermore, the hardness of the CuNiFe-5 wt.%W alloys numbers (5–8) B through the (W, Fe) powder pre-milling using planetary ball milling, as shown in Table 4. The hardness at 79 and 85 HV for 0.5 and 4.0 h (W, Fe) pre-milling time was obtained, respectively. It is clearly observed that the CuNiFe alloys with 5.0 wt.% W shows a higher hardness through (W, Fe) pre-milling. This fact might be correlated with the reduced crystallite size of the (W, Fe) elements and homogenous distribution within the microstructure of the alloy, as shown in Figures 3 and 9. It is believed that there is a strong correlation between the finer and uniform distribution of particles acting as dislocation barriers and their ultimate contribution to the strength of the alloys. The mechanical properties improvement of Cu-Ni-Sn-P alloy due to finer and uniform distribution of particles of precipitate formation was also reported [33].

Furthermore, Table 4 displays the compressive strength of CuNiFe-xW alloys, demonstrating an enhancement in compressive yield strength with the incorporation of the W element. The presence of a small amount of W can act as a precipitate that impedes dislocation movement and further increases the strength [34]. The increase of this element tends to reduce the ductility of the model CuNiFe-xW alloys. This work reveals that the presence of the W element induces the formation of the W-oxides phase in sintered CuNiFe-5 wt.%W alloys, as confirmed by XRD analysis (refer to Figure 10). The large size, excessive particle, and non-homogeneous distribution of these oxide particles within the microstructure could be detrimental to the ductility of model alloys. In contrast, the dispersion strengthening process is responsible for the enhanced strength and ductility seen in Cu-Cr alloys when nano oxide particles are uniformly distributed throughout them [35]. The (W, Fe) powder pre-milling increases the yield strength of CuNiFe-5 wt.%W from 172 to 203 MPa and also improves compressive strength to 784 MPa

Table 4. The mechanical properties of a varying model CuNiFe-xW-based alloy

Alloys num-ber	Alloy designation	Vickers hardness		Yield strength			Compressive strength		
		(HV)	Std. deviation	(MPa)	Std. deviation	Strain (%)	(MPa)	Std. deviation	Strain (%)
1-A	CuNiFe-1wt.%W	66	± 2.6	141	± 9.8	6.3	208	± 19.6	26.0
2-A	CuNiFe-3wt.%W	71	± 2.7	163	± 8.5	6.0	284	± 25.5	25.6
3-A	CuNiFe-5wt.%W	77	± 0.7	169	± 4.6	5.9	307	± 18.2	24.7
4-A	CuNiFe-7wt.%W	83	± 2.7	184	± 3.0	5.9	351	± 13.2	23.6
5-B	CuNiFe-5wt.%W-P0	79	± 1.0	172	± 20.1	5.6	662	± 48.3	35.0
6-B	CuNiFe-5wt.%W-P1	80	± 0.4	180	± 9.2	4.3	651	± 56.8	34.0
7-B	CuNiFe-5wt.%W-P2	83	± 2.6	190	± 23.1	4.9	720	± 59.7	32.0
8-B	CuNiFe-5wt.%W-P4	85	± 3.7	203	± 25.1	4.9	784	± 56.2	29.0

for a 4.0 h pre-milling time (Table 4). In the yield strength areas, the model CuNiFe-xW alloys deformed plastically, and some cracks or fractures can be observed on the alloy's surface.

Figure 11 shows the fracture morphologies of the CuNiFe-xW alloy observed by the SEM method. A small shallow dimple in the CuNiFe-5 wt.%W with 4.0 h (W, Fe) powder pre-milling was observed in the fracture areas. More dimple fracture areas with microporosities were also observed in the CuNiFe-7 wt.%W fracture areas, which confirmed ductile fracture of the alloy as shown in Figure 11b. The existence of pores reduces the ductility of these alloys, even when dimple fractures are still visible. There is a robust relationship between pore fractions and mechanical qualities, including ductility and fracture toughness, which makes them essential [36]. The pore defects in the microstructure influence the increase in the stress concentration and failure of the material [37]. In certain spots, a microscale brittle fracture model alloy was seen; nevertheless, these cracks also proved that the model alloy predominantly showed ductile fracture with dimple regions, perhaps because the matrix was made of Cu and Ni elements.

The fracture areas of the CuNiFe-1.0 wt.%W exhibit elongated grains, with fracture initiation occurs through the formation of small cracks across the grain that promote transgranular fracture, as illustrated in Figure 12a-b. These fracture models confirmed that the model alloy has good ductility, aligning with the increased strain as shown in Table 4. Furthermore, Figure 12a shows the micro-porosity defects and flat fracture surface dispersed throughout the fracture area. The existence of these defects and impurities at the grain boundary is believed to significantly contribute to crack formation and diminish the fracture toughness of model CuNiFe-based alloys. Meanwhile, Figure 12b illustrates the magnification of the chosen fracture region; it is evident that the Cu-rich zone, designated as

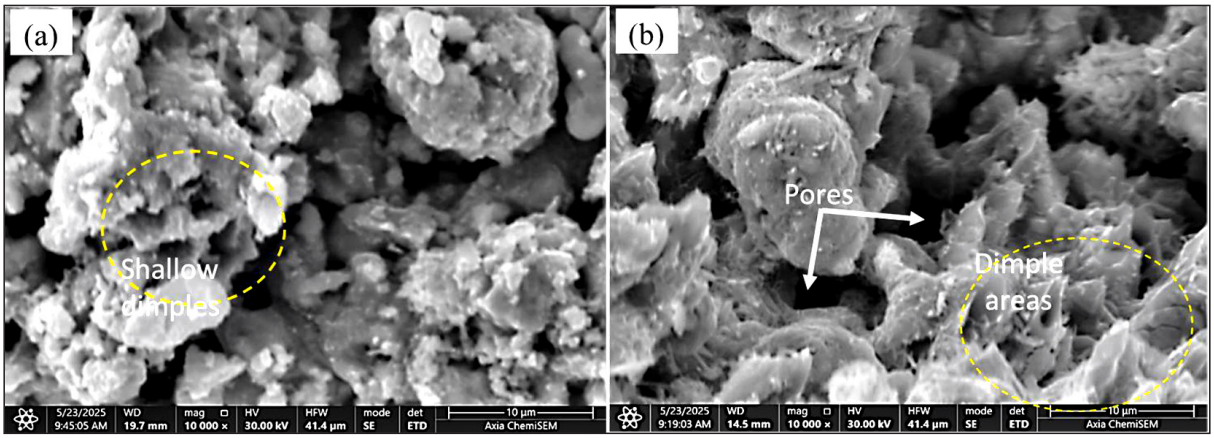

Figure 11. The fracture morphologies of the model (a) CuNiFe-5wt.%W-P4 alloy subjected to 4.0 h (W, Fe) powder pre-milling and (b) CuNiFe-7wt.%W alloy without pre-milling

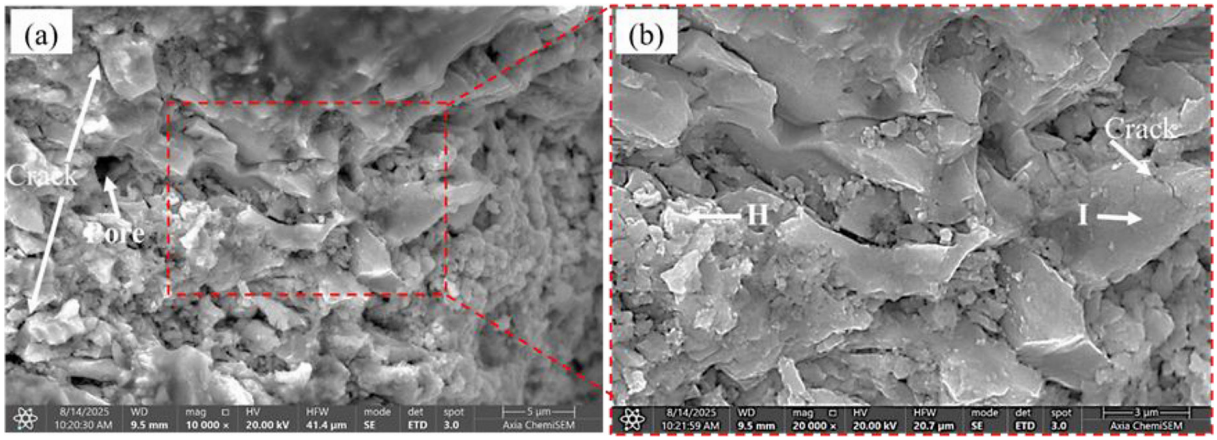

Figure 12. The fracture morphologies of the (a) CuNiFe-1.0 wt.%W model alloy and (b) enlarged rectangle area

Table 5. The constituent elements in the selected fracture area of the CuNiFe-1 wt.%W alloy

Selected area	Elements				
	Cu	Ni	Fe	W	O
H	18.3	0.6	68.3	-	12.8
I	58.8	0.4	28.1	0.2	12.5

a gray area, underwent deformation and initiated a microcrack prior to fracture.

The constituent elements in some fracture areas, such as points H and I, were characterized by EDS point, as demonstrated in Table 5. Point-H, with a light gray and flat fracture, exhibits a predominant composition of 68.3 wt.% and 18.3 wt.% for Fe and Cu elements as the main elements in this model CuNiFe-1.0 wt.%W alloys. In this area (Point-H), 12.8 wt.% O elements were also detected, which is due to they have good affinity with Fe, suggesting that this area might be some Fe-oxide formed during high-temperature sintering. In the other area (Point-I), a significant presence of 58.8 wt.% Cu accompanied by 28.1 wt.% Fe was observed, confirming that the FCC matrix is predominantly present in this area. However, the presence of W (0.2 wt.%) and O (12.5 wt.%) in this region suggests the potential formation of W/Fe-oxide within the FCC solid solution phases. A non-homogeneous distribution of elements was detected in the fracture regions at a micro-scale level. These results are consistent with the EDS point of the designated area of sintered alloys, as illustrated in Table 2.

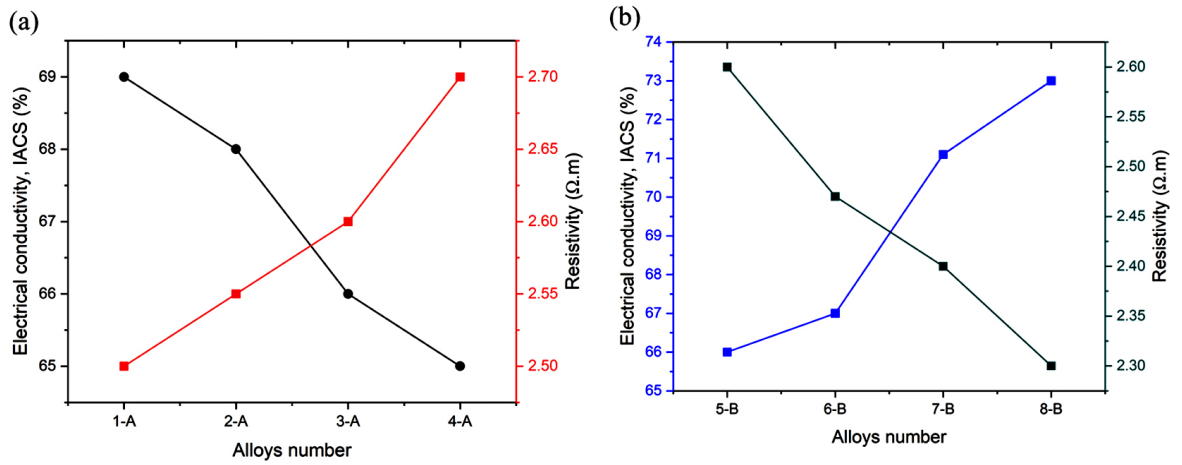

Figure 13. The electrical properties of the (a) CuNiFe-x wt.%W with varying W and (b) CuNiFe-5 wt.%W with different (W, Fe) pre-milling time

The electrical properties of the sintered CuNiFe-xW alloy

Figure 13 shows the electrical conductivity of the CuNiFe-xW model alloys; the augmentation of W in Cu-Ni-Fe diminishes the electrical conductivity, leading to a reduction (±5.7%) from 69 to 65% IACS. The reason behind, is that W has a lower conductivity compared to the Cu matrix, but the resistance grows as the W element concentration increases. This finding is in line with another study that suggests that electrical conductivity is decreased when Cr is added to Cu, but electrical characteristics are improved when annealing is introduced [22]. In this current study, the (W, Fe) powder pre-milling exhibits enhanced electrical conductivity, showing a linear increase with the highest conductivity of 73% IACS and the lowest resistivity of 2.3 Ω·m for the model CuNiFe-5 wt.%W alloy after 4.0 h of powder pre-milling. These results confirmed that the (W, Fe) pre-milling successfully improved the electrical properties, which correspond well with the mechanical properties. It is believed that the properties improvement is correlated with finer (W, Fe) particles, which generate a more homogeneous distribution of W in the microstructure and less porosity, as shown in Figures 9 and 6, respectively. The porosity significantly affects electrical conductivity, as it acts as an insulator barrier to electron movement within the Cu-matrix, in which the increase of the porosity reduces conductivity [25].

CONCLUSIONS

The role of the W element and (W, Fe) powder pre-milling on the characteristics of CuNiFe-xW alloys was analyzed by using various methods. Several conclusions can be drawn from the data. The incorporation of W up to 7.0 wt.% effectively enhanced the hardness and compressive strength, achieving the maximum of 83 HV and 184 MPa, respectively. The W can act as a barrier to dislocation movement and enhance the strength of the model alloys. On the other hand, the (W, Fe) powder pre-milling improved the hardness of CuNiFe-5 wt.%W, from 79 HV without pre-milling to 85 HV with (W, Fe) powder pre-milling. The highest yield strength of 203 MPa was attained for 4.0 h of (W, Fe) powder pre-milling. The (W, Fe) pre-milling process facilitated a more uniform microstructure and elemental distribution in the sintered model CuNiFe-5 wt.%W alloys. However, the addition of the W reduces the electrical conductivity of Cu-Ni-based alloy, with the lowest 65% IACS and the highest 73% IACS for 4.0 h (W, Fe) powder pre-milling times. These results contribute to the scientific field by developing a two-stage powder mixing method to enhance the mechanical and electrical properties of the alloys. Based on the data, the electrical conductivity above 50% IACS has the potential to be used as a material candidate in the electrode component.

Acknowledgements

The authors would like to thank the Directorate of Research and Community Service (Indonesian: Direktorat Penelitian dan Pengabdian kepada Masyarakat/DPPM) of the Ministry of Higher Education, Science, and Technology of the Republic of Indonesia, for providing financial support for this current study under contract No. 46/UN5.4.10.K/PT.01.03/DPPM/2025

REFERENCES

1. Akhyar A., Zulfadhli, Ali N., Arhami, Huzni S., Maulana R. Effect of superheat on hot tearing susceptibility in re-melted 6061 aluminum alloy. Int. J. Metalcast. 2025, 19, 2788–2805. https://doi.org/10.1007/s40962-024-01498-z
2. Zulfadhli, Akhyar A, Ali N., Arhami, Pahlevi M.R. Variations in casting temperatures effect of re-melted 6061 aluminum alloy on tensile strength. Results Mater. 2025, 26, 1–11. https://doi.org/10.1016/j.rinma.2025.100691
3. Kargul M. Influence of the type of strengthening particles on the tribological and material properties of sintered copper matrix composites. ASTRJ. 2025, 19, 19–33. https://doi.org/10.12913/22998624/205674
4. Nnakwo K.C. Effect of tungsten content on the structure, physical and mechanical properties of silicon bronze (Cu-3 wt%Si). J. King Saud Univ. Sci. 2019, 31, 844–848. https://doi.org/10.1016/j.jksus.2017.12.002
5. Stąpór S, Górny M., Gondek Ł., Gracz B. The role of molybdenum in the formation of the microstructure and properties of Al-Cu alloys. Arch. Foundry Eng. 2024, 24, 39–48. https://doi.org/10.24425/afe.2024.151308
6. Haußmann L., Rehman H.U., Matschkal D., Göken M., Neumeier S. Solid solution strengthening of Mo,

Re, Ta and W in Ni during high-temperature creep. Metals. 2021, 11, 1–8. https://doi.org/10.3390/met11121909

7. Mohammed M.M., Alrasheedi N.H., El-Kady O.A., Djuansjah J., Essa F.A., Elsheikh A.H. Impact of using tungsten, cobalt, and aluminum additives on the tribological and mechanical properties of iron composites. Crystals. 2023, 13, 1–14. https://doi.org/10.3390/cryst13030395
8. Yusoff M., Zuhailawati H. In situ tungsten carbide formation in nanostructured copper matrix composite using mechanical alloying and sintering. Materials. 2022, 15, 1–13. https://doi.org/10.3390/ma15072340
9. Sukhova O.V. The effect of iron on precipitation hardening in the Cu-Ni-Mn alloys. Phys. Chem. Solid St. 2021, 22, 487–493. https://doi.org/10.15330/pcss.22.3.487-493
10. Suprianto, Maulana F.P., Prasetyo S.B., Sabri M., Suherman, Ichwani R. Effect of iron content and warm compaction temperature on microstructure evolution and characteristics of the Cu-Ni-xFe based alloys. ASTRJ. 2025, 19, 12–26. https://doi.org/10.12913/22998624/197042
11. Wang M., Yang Q. R., Jiang Y. B., Li Z., Xiao Z., Gong S., Wang Y.R., Guo C.L., Wei H.G. Effects of Fe content on microstructure and properties of Cu–Fe alloy. Trans. Nonferrous Met. Soc. China. 2021, 31, 3039–3049. https://doi.org/10.1016/S1003-6326(21)65713-8
12. Yuan X., Zhang P., Wang J., Yang B., Li Y. Influences of Fe content and cold drawing strain on the microstructure and properties of powder metallurgy Cu-Fe alloy wire. Materials. 2023, 16, 1–13. https://doi.org/10.3390/ma16145180
13. Marković I., Trujić S., Manasijević D., Balanovic L., Stamenković U., Mitrović M. Effect of particle shape and size of copper powders on the properties of sintered parts. J. Sustain. Technol. Mater. 2023, 3, 22–29. https://doi.org/10.57131/jstm.2023.4.4
14. Sankhla A.M., Patel K.M., Makhesana M.A., Giasin K., Pimenov D.Y., Wojciechowski S., Khanna N. Effect of mixing method and particle size on hardness and compressive strength of aluminium based metal matrix composite prepared through powder metallurgy route. J. Mater. Res. Technol. 2022, 18, 282–292. https://doi.org/10.1016/j.jmrt.2022.02.094
15. Lee S.J., Hwang S.Y. Comparative study to evaluate mixing efficiency of very fine particles. Appl. Sci. 2025, 15, 1–29. https://doi.org/10.3390/app15158712
16. Lebedev M., Promakhov V., Schulz N., Vorozhtsov A., Lerner M. Effects of sintering temperature on the microstructure and properties of a W-Cu pseudo-alloy. Metals. 2023, 13. https://doi.org/10.3390/met1310174
17. Arora A., Kumar A., Mula S. Effect of Y_2O_3 on mechanical and corrosion properties of Fe and Fe-Ni alloys prepared by mechanical alloying followed by spark plasma sintering. J. Mater. Eng. Perform. 2021, 30, 1387–1397. https://doi.org/10.1007/s11665-020-05356-x
18. Lucas F.M., Trindade B., Costa B.F.O., Le Caër G. Mechanical Alloying of Fe-Cu Alloys from As-received and premilled elemental powder mixtures. Key Eng. Mater. 2002, 230–232, 631–632. https://doi.org/10.4028/www.scientific.net/KEM.230-232.631
19. Shang X., Wang X., Chen S. Effects of ball milling processing conditions and alloy components on the synthesis of Cu-Nb and Cu-Mo alloys. Materials. 2019, 12, 1–9. https://doi.org/10.3390/ma12081224
20. Yakovtseva O.A., Emelina N.B., Mochugovskiy A.G., Tabachkova. N., Tabachkova A.S., Mikhaylovskaya A.V. Influence of pre-milling on the Mn solid solubility in the Al-Mn-Cu alloy during mechanical alloying. Metals. 2023, 13,1–14. https://doi.org/10.3390/met13040756
21. Oboso P.B., Oyama S., Horioka J., Yi L.F., Onda T., Morito S., Chen Z.C. Microstructure and mechanical properties of CuCrFeNi medium entropy alloys synthesized via mechanical alloying and spark plasma sintering. J. Alloys Compd. 2025, 1010, 1–11. https://doi.org/10.1016/j.jallcom.2024.177700
22. Uchida S, Kimura T, Nakamoto T, Ozaki T., Miki T., Takemura M., Oka Y., Tsubota R. Microstructures and electrical and mechanical properties of Cu-Cr alloys fabricated by selective laser melting. Mater. Des. 2019, 175, 1–10. https://doi.org/10.1016/j.matdes.2019.107815
23. Wu Z., Liang Y., Fu E., Du J., Wang P., Fan Y., Zhao Y. Effect of ball milling parameters on the refinement of tungsten powder. Metals. 2018, 8, 1–13. https://doi.org/10.3390/met8040281
24. Adam O., Jan V. Influence of Milling Time on the Microstructure of Immiscible Cu-Fe-Co-W Alloy Prepared by Powder Metallurgy. 29th International Conference on Metallurgy and Materials. Brno, Czech Republic, May 20–22 2020, 1092–1097. https://doi.org/10.37904/metal.2020.3613
25. Houssain H., Cengiz A.O., Islak S. Effect of mechanical alloying time on microstructure, hardness and electrical conductivity properties of Cu-B4C composites. KUJES. 2024, 7–4. https://doi.org/10.55385/kastamonujes.1449504
26. Biyik S., Aydin M. Optimization of mechanical alloying parameters of Cu25W electrical contact material. Acta Phys Pol A. 2017, 132, 909–912. https://doi.org/10.12693/APhysPolA.132.909
27. Suprianto, Chen C.L. Study of Cu effect and in-situ yttria dispersoids on microstructure evolution

of mechanically alloyed CoFeNiCrCu high entropy alloys. Met. Mater. Int. 2023, 29, 420–428. https://doi.org/10.1007/s12540-022-01258-w

28. Jones B., Tse Lop Kun J., Patterson E., Allapat N., Atwater M. Hybrid pore formation in copper spheres by gas entrapment and oxide reduction. Adv. Eng. Mater. 2024, 26, 1–12. https://doi.org/10.1002/adem.202301198
29. Divinski S., Ribbe J., Schmitz G., Herzig C. Grain boundary diffusion and segregation of Ni in Cu. Acta Mater. 2007, 55, 3337–3346. https://doi.org/10.1016/j.actamat.2007.01.032
30. Gezerman A.O., Çorbacioğlu B.D. Effects of mechanical alloying on sintering behavior of tungsten carbide-cobalt hard metal system. Adv. Mater. Sci. Eng. 2017, 1–11. https://doi.org/10.1155/2017/8175034
31. Agus J., Samnur S., Triyana K., Sujiono E.H. Effect of sintering temperature on crystal structure and surface morphology of $NdFeO_3$ oxide alloy materials prepared by solid reaction method. Key Eng. Mater. 2019, 811, 158–162. https://doi.org/10.4028/www.scientific.net/KEM.811.158
32. Song B., Yu T., Jiang X., Xi w., Lin X. Effect of W content on the microstructure and properties of Cu-Fe alloy. J. Mater. Res. Technol. 2020, 9, 6464–6474. https://doi.org/10.1016/j.jmrt.2020.04.031
33. Chen X., Xiao X., Yuan D., Chen J., Wu Y. Effect of Ni/Sn ratio on microstructure and properties of Cu-Ni-Sn-P alloy. Sci. Rep. 2024, 14, 1–11. https://doi.org/10.1038/s41598-024-80079-w
34. Zhao J., Lee T., Lee J.H., Jiang Z., Lee C.S. Effects of tungsten addition on the microstructure and mechanical properties of microalloyed forging steels. Metall Mater Trans A Phys Metall Mater Sci. 2013, 44, 3511–3523. https://doi.org/10.1007/s11661-013-1695-x
35. Zhou Y., Yin S., Lei Q., Fan J., Wei S., Yan Y. The synchronous improvement of thermal stability, mechanical properties, thermal conductivity of oxide dispersion strengthened Cu–Cr alloy by microalloying Si. J. Mater. Res. Technol. 2025, 34, 2161–2173. https://doi.org/10.1016/j.jmrt.2024.12.212
36. Toda H., Inamori T., Horikawa K., Uesugi K., Takeuchi A., Suzuki Y., Kobayashi M. Effects of hydrogen micro pores on mechanical properties in a2024 aluminum alloys. Mater. Trans. 2013, 54, 2195–2201. https://doi.org/10.2320/matertrans.L-M2013832
37. Zhang W., Liu J., Xing Y., Ao X., Yang R., Yang C., Tan J. Effects of pore defects on stress concentration of laser melting deposition-manufactured AlSi10Mg via crystal plasticity finite element method. Materials. 2025, 18. https://doi.org/10.3390/ma18102285